Instabilities in the flow past localized magnetic fields

Alberto Beltrán, Sergio Cuevas

Centro de Investigación en Energía, UNAM, A.P. 34, Temixco, Morelos, 62580 MEXICO

E-mail: albem@cie.unam.mx, scg@cie.unam.mx

Sergey Smolentsev

Mechanical and Aerospace Engineering Department, UCLA, 44-114 Engineering IV, Los Angeles, CA 90095-1597, USA

E-mail: sergey@fusion.ucla.edu

Abstract. The flow in a shallow layer of an electrically conducting fluid past a localized magnetic field is analyzed numerically. The field occupies only a small fraction of the total flow domain and resemblances the magnetic field created by a permanent magnet located close to the fluid layer. Two different physical cases are considered. In the first one, the fluid layer is free from externally injected electric currents, therefore, only induced currents are present. In the second case, an external electric current is injected to the fluid layer, transversally to the main flow direction. It is shown that the Lorentz force created by the interaction of the electric currents with the non-uniform magnetic field acts as an obstacle for the flow and creates different flow patterns similar to those observed in the flow past bluff bodies. A quasi-two-dimensional model that takes into account the existence of the bottom wall through a linear Hartmann-Rayleigh friction term is considered. When inertial and magnetic forces are strong enough, the wake formed behind the zone of high magnetic field is destabilized and a periodic vortex shedding similar to the classical von Kármán street is found. The effect of Hartmann-Rayleigh friction in the emergence of the instability is analyzed.

1. Introduction

There is a practical interest to investigate magnetohydrodynamic (MHD) flows that may become unstable and present a time-dependent behavior. In fact, promotion of unsteady inertial flows, in particular time-dependent mixing, is desirable for heat transfer enhancement purposes. In spite of some stabilizing effects of steady magnetic fields, there are several MHD flows at low magnetic Reylods number that may present unstable behavior. For instance, high velocity side layer flows in rectangular ducts [1, 2], flows past solid obstacles [3, 4], flows in ducts with non-uniform wall conductance [5, 6], electrically driven flows [7, 8], and flows in localized magnetic fields [9, 10, 11, 12], provide examples of the appearance of instabilities in flows of conducting liquids under steady magnetic fields.

In general, an external magnetic field affects the stability of a base flow of an electrically conducting fluid in two opposite ways. In the one hand, there is an *stabilizing effect* produced by two mechanisms: the damping of velocity fluctuations by Joule dissipation and the braking of the flow by the Hartmann effect. The damping of fluctuations manifests the dissipative action of electric currents circulating in the fluid, since kinetic energy is converted into heat via Joule

dissipation. In MHD flows, Joule dissipation leads to a more rapid damping of disturbances than in flows where only viscous dissipation prevails. Besides, the circulation of electric currents in boundary layers attached to walls where a normal component of the applied magnetic field exists, creates a Lorentz force that tends to brake the fluid motion (i.e the *Hartmann braking*). Since velocity gradients are increased near the wall, wall friction is also increased, leading to a rise in the drag coefficient. As a matter of fact, the possibility of flow stabilization through the action of a steady magnetic field, is the basis of many technological applications [13].

On the other hand, Lorentz forces may also produce a *destabilizing effect* on the flow by modifying the mean-flow velocity distribution. In fact, the creation of inflection points in the velocity profile is the mechanism by which Lorentz forces may reduce the stability of the flow. There are several examples that show the emergence of instabilities when non-uniformities in the electromagnetic conditions of the flow are present. Non-uniformities, for instance, in the electrical conductivity of the walls or in the strength of the magnetic field, promote the creation of internal shear layers. However, the presence of non-negligible intertial effects is a necessary condition for these layers to become unstable. This is shown very clearly in the paper by Bühler [6] where the quasi-two-dimensional flow in a duct with a discontinuity in the electrical conductivity of the walls under a uniform magnetic field, was theoretically analyzed. He showed that inhomogeneity in the wall conductivity may develop an instability that leads to time-dependent solutions similar to the Kármán vortex street behind bluff bodies. In fact, the formation of a Kármán street was also observed experimentally in the shallow flow of mercury in an insulating open channel in which a copper disk much thinner than the fluid depth was mounted on the bottom [5]. Non-uniform magnetic fields may also be the source of flow instabilities. Arranges of permanent magnets have long been used to promote mixing and even to get quasi-two-dimensional turbulent regimes by injecting electric currents in thin fluid layers [7, 8]. A less studied stuation involves the creation of internal shear layers by traveling localized magnetic fields in quiescent fluids or, equivalently, uniform flows past fixed localized fields. As a matter of fact, flows of this kind exhibit some features similar to those of ordinary flows around solid obstacles. It has been shown experimentally that vortical flows can be generated by the interaction of the field produced by a traveling permanent magnet, with an electric current applied through a thin layer of an electrolyte [9, 10, 11]. Depending on the velocity of the magnet and the injected electric current, different flow patterns can be generated, including a wavy wake, symmetric vortex pairs and even periodic vortex shedding. Recently, the interaction of a uniform flow with a localized magnetic field, denominated a *magnetic obstacle*, was analyzed numerically considering that inertial effects dominate over *Hartmann-Rayleigh friction* in the bounday layers attached to the bottom wall [12]. Unlike experimental studies, no injected electric currents were considered and Lorentz forces were created instead by the interaction of induced electric currents with a localized field. It was shown that this field acts as an obstacle for the flow and, under certain conditions, an instability leading to vortex shedding can appear. In the present contribution, we extend the previous study by assessing numerically the effect of Hartmann-Rayleigh friction in the emergence of the instability, in a thin layer of conducting fluid. Further, preliminary simulations of flows induced by injected currents are also considered.

2. Formulation

Let us consider the flow of a thin layer of an electrically conducting incompressible viscous fluid under the influence of a non-uniform magnetic field, produced by a localized source. At the bottom, the fluid is bounded by an electrically insulated rigid wall, and at the top, by a free surface. Lateral boundaries are assumed to be far enough from the magnetic source, so that their influence on the flow in the neighborhood of the source is negligible. The magnetic field is produced by a square magnetized surface uniformly polarized in the normal direction, embedded

on the bottom wall. Since its magnetic dipole moment points in the direction normal to the plane of flow (positive z-direction), the dominant contribution of the applied field comes from the normal component and is the only one considered. If we place the coordinate system in the centre of a rectangular surface with side lengths $X_0 = 2a$ and $Y_0 = 2b$, the normal component of the field produced by a single magnetized surface laying on the plane $Z = -h$ is given in dimensional terms by [14]

$$\begin{aligned}\mathcal{B}_z^0 &= \gamma B_{max}\left\{\tan^{-1}\left(\frac{(X+a)(Y+b)}{(Z-Z_0)[(X+a)^2+(Y+b)^2+(Z-Z_0)^2]^{1/2}}\right)\right.\\ &+\tan^{-1}\left(\frac{(X-a)(Y-b)}{(Z-Z_0)[(X-a)^2+(Y-b)^2+(Z+h)^2]^{1/2}}\right)\\ &-\tan^{-1}\left(\frac{(X+a)(Y-b)}{(Z-Z_0)[(X+a)^2+(Y-b)^2+(Z+h)^2]^{1/2}}\right)\\ &\left.-\tan^{-1}\left(\frac{(X-a)(Y+b)}{(Z-Z_0)[(X-a)^2+(Y+b)^2+(Z+h)^2]^{1/2}}\right)\right\}, \qquad (1)\end{aligned}$$

where $\mathcal{B}_z^0$ stands for the dimensional applied magnetic field and γ is a normalization constant. For the sake of simplicity, we consider that the magnetized surface has a square shape, that is, $2a = 2b = L$, where L is taken as the characteristic length of the flow. It is assumed that the size of the magnetized surface is small compared to the whole flow region; consequently, the non-uniform magnetic field affects only a small localized zone. Since the surface is embedded on the bottom wall, h corresponds to the thickness of the fluid layer. We assume that the applied magnetic field is an independent function of the z-coordinate. Actually, the variation of the applied field in the normal direction is slight since the thickness of the layer is small compared to the length of the flow domain in the $x-$ and $y-$directions.

Far from the magnetic source, the fluid displays a uniform flow of magnitude U in the positive x-direction. The motion of the fluid within the applied field induces electric currents which generate an induced field $\mathbf{b}$, so that the total magnetic field is given by $\mathbf{B} = \mathbf{B}^0 + \mathbf{b}$. We assume that the induced field is much smaller than the applied field, $\mathbf{b} << \mathbf{B}^0$, which means that the magnetic Reynolds number, $Rm = \mu\sigma UL$, is much less than unity. Here, μ and σ, are the magnetic permeability and the electrical conductivity of the fluid, respectively. We consider two different physical situations. In the first one, the fluid layer is free from externally injected electric currents, therefore, only induced currents are present. The induced currents interact with $\mathbf{B}$ giving rise to a non-uniform Lorentz force that opposes the oncoming flow and creates vorticity. In the second situation, we consider that, besides induced currents, an external electric current is injected to the fluid layer, transversally to the main flow direction. In fact, the current is injected in the negative y-direction so that the created Lorentz force, as well as the induced Lorentz force, opposes the oncoming flow. Evidently, in this case, the superposition of forces lead to stronger opposing force.

It is important to note that the generation of vorticity by Lorentz forces and the stability of the flow are strongly influenced by the uniformity or non-nuniformity of the applied magnetic field. The generation of vorticity can be analyzed by looking at the curl of the Lorentz force, namely, $\nabla\times(\mathbf{j}\times\mathbf{B}^0) = (\mathbf{B}^0\cdot\nabla)\mathbf{j}+(\mathbf{j}\cdot\nabla)\mathbf{B}^0$, where $\mathbf{j}$ denotes the induced electric current density. In flows under uniform fields, induced currents form cross-sectional loops (in planes parallel to the applied field) that close through Hartmann layers. In this case, the vorticity is generated by the term $(\mathbf{B}^0\cdot\nabla)\mathbf{j}$. Further, Hartmann braking generated due to currents closing through Hartmann layers tend to stabilize the flow. On the other hand, under non-unifrom fields, electric currents form loops in both planes parallel and perpendicular to $\mathbf{B}^0$ and the term $(\mathbf{j}\cdot\nabla)\mathbf{B}^0$ strongly contributes to the vorticity generation. In fact, current loops in planes perpendicular to $\mathbf{B}^0$ can

modify dramatically the velocity distribution and affect the flow stability.

In the next Section, we consider flows in the absence of injected electric currents, and analyze the effect of bottom friction in the stability of the flow. In Section 4, injected electric currents are considered.

3. Flow in the absence of injected electric currents

Since a significant geometrical confinement is imposed by the small thickness of the fluid layer, we consider that the flow is quasi-two-dimensional. With a quasi-two-dimensional approach, the problem is usually formulated in terms of core variables, but the effect of the boundary layers is still included through an additional term on the momentum equation accounting for the wall friction. In this way, we reduce the computational effort of solving a three-dimensional problem to a two-dimensional flow formulation for the core variables. In order to do that, we integrate (average) the equations in the normal direction. This has been done in the past in flows under uniform magnetic fields [6, 15] as well as under a non-uniform field [16]. Recently, this approach was used for analyzing flows under localized magnetic fields [12].

Following the quasi-two-dimensional approach, we assume that the transport of momentum in the normal direction is mainly diffusive so that the velocity components can be expressed in the form

$$u(x,y,z,t) = \overline{u}(x,y,t)f(x,y,z), \quad v(x,y,z,t) = \overline{v}(x,y,t)f(x,y,z), \tag{2}$$

where $\overline{u}$ and $\overline{v}$ are the velocity components in the x and y directions, respectively, averaged in the normal direction (core variables), and the function f considers the variation of the velocity profile in this direction. Its dependence on x and y coordinates must reflect the different flow regions due to the localization of the magnetic field. The function f must satisfy non-slip conditions at the bottom wall, and stress free condition at the free surface. In addition, f must also satisfy the normalization condition, namely, $\int_0^\alpha U f dz = \alpha$, where $\alpha = h/L$ is the aspect ratio or the dimensionless layer thickness. In dimensionless terms, we assume that the function f is given by

$$f = \frac{\alpha \mathcal{H}a}{\alpha \mathcal{H}a - \tanh(\alpha \mathcal{H}a)} \left[(1 - e^{\mathcal{H}az}) + e^{\alpha \mathcal{H}a} \frac{\sinh(\mathcal{H}az)}{\cosh(\alpha \mathcal{H}a)} \right] \tag{3}$$

where $\mathcal{H}a(x,y) = HaB_z^0$ is the *local* Hartmann number. The parameter Ha is the ordinary Hartmann number, defined as $Ha = B_{max}L\sqrt{\sigma/\rho\nu}$, where ρ and ν are the mass density and the kinematic viscosity of the fluid, respectively. In turn, B_z^0 is the dimensionless expression of the applied field (1), normalized by B_{max}. Coordinates x, y, and z are normalized by L. The expression (3), reproduces the ordinary Hartmann flow profile in the region where the magnetic field is intense and becomes a parabolic profile in regions where the magnetic field is negligible.

We use the assumption (2) and Eq. (3) for averaging the governing MHD equations [12], by integrating in the normal direction from the bottom wall to the free surface. The dimensionless averaged equations of motion in the absence of injected electric currents take the form

$$\frac{\partial u}{\partial x} + \frac{\partial v}{\partial y} = 0, \tag{4}$$

$$\frac{\partial u}{\partial t} + \left(u\frac{\partial u}{\partial x} + v\frac{\partial u}{\partial y} \right) K = -\frac{\partial P}{\partial x} + \frac{1}{Re}\nabla_\perp^2 u - \frac{u}{\tau} + \frac{Ha^2}{Re} j_y B_z^0, \tag{5}$$

$$\frac{\partial v}{\partial t} + \left(u\frac{\partial v}{\partial x} + v\frac{\partial v}{\partial y} \right) K = -\frac{\partial P}{\partial y} + \frac{1}{Re}\nabla_\perp^2 v - \frac{v}{\tau} - \frac{Ha^2}{Re} j_x B_z^0, \tag{6}$$

where the overline in the velocity components has been dropped and the subindex $\perp$ denotes the projection of the ∇ operator on the $(x-y)$-plane. In addition, the velocity $\mathbf{u}$, the pressure p, and the electric current density $\mathbf{j}$, are normalized by U, ρU^2, and $\sigma U B_{max}$, respectively, while the time t is normalized by L/U. The parameter $Re = UL/\nu$ is the Reynolds number. The factor K stands for the integral $\frac{1}{\alpha}\int_0^\alpha f^2 dz$, which explicitly becomes

$$K = \frac{\frac{\alpha\mathcal{H}a}{2}\left[\alpha\mathcal{H}a\left(2+\frac{1}{\cosh^2(\alpha\mathcal{H}a)}\right)-3\tanh(\alpha\mathcal{H}a)\right]}{(\tanh(\alpha\mathcal{H}a)-\alpha\mathcal{H}a)^2}. \tag{7}$$

Figure 1(a) shows K as a function of the axial coordinate for different Hartmann numbers, assuming that the center of the magnetized plate is located at $x = 0$, $y = 0$. Note that it deviates slightly from unity, so that this factor does not alter substantially the convective terms. The third term in equations (5) and (6) represents the Hartmann-Rayleigh friction [12] due to the existence of boundary layers attached to the bottom wall. This term models the magnetic (Hartmann) friction in the zone of high magnetic field strength or the viscous (Rayleigh) friction in zones where the magnetic field is negligible. It involves a characteristic timescale, τ, for the decay of vorticity due to dissipation in the Hartmann and viscous layers. The inverse of this timescale is given by

$$\tau^{-1} = \frac{1}{\alpha Re}\frac{\partial f}{\partial z}\,|_0^\alpha = \frac{\mathcal{H}a^2}{Re}\frac{\tanh(\alpha\mathcal{H}a)}{\alpha\mathcal{H}a-\tanh(\alpha\mathcal{H}a)}. \tag{8}$$

In fact, τ is the ratio of a typical eddy turnover time and a typical time scale for the Hartmann braking [12]. It can be shown that in the limit $\mathcal{H}a \to 0$ (which occurs outside the region of strong magnetic field) this coefficient becomes the inverse of a viscous diffusion time. In figure 1(b), τ^{-1} is shown as a function of the x-coordinate for different Hartmann numbers. It can be observed that the friction is maximum at the origin where the magnetic field strength is also maximum, and decays to a constant (viscous) value as the distance from the origin grows. Also, τ^{-1} grows in the obstacle region as the Hartmann number grows, and decreases as α decreases. This means that the friction is increased the stronger the magnetic field and the thinner the layer thickness.

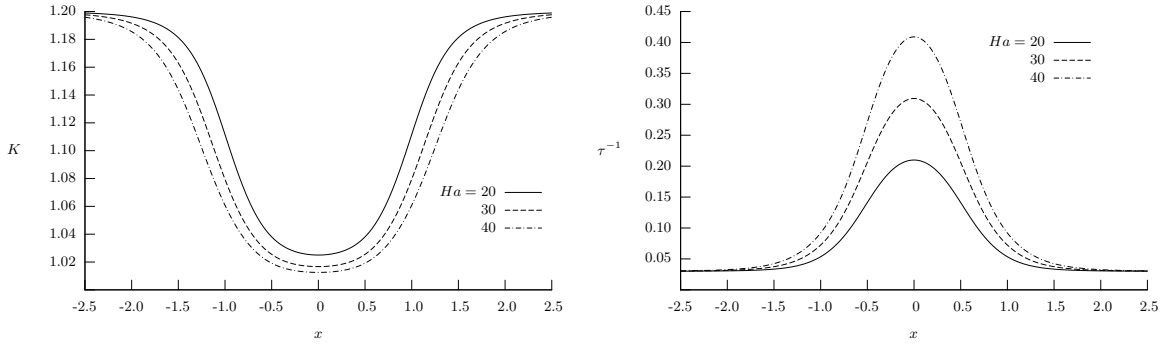

Figure 1. (a) Function K versus axial coordinate for different Hartmann numbers. (b) Inverse of characteistic time scale versus the axial coordinate. $\alpha = 1$

In order to close the system of equations (4)-(8), we have to consider the induction equation in the quasi-static approximation. It reduces to a single equation for the component b_z:

$$\nabla_\perp^2 b_z - u\frac{\partial B_z^0}{\partial x} - v\frac{\partial B_z^0}{\partial y} = 0. \tag{9}$$

The current density components are calculated from Ampère's law in the form

$$j_x = \frac{\partial b_z}{\partial y}, \qquad j_y = -\frac{\partial b_z}{\partial x}. \tag{10}$$

3.1. Numerical implementation

We look for numerical solutions using a formulation based on the primitive variables, the velocity and pressure, and the induced magnetic field as electromagnetic variable. A finite difference method on an orthogonal equidistant grid was used to solve the governing Eqs. (4)–(9) under suitable boundary conditions, assuming a motionless fluid as initial condition. The standard time-marching procedure described in [17] was extended to consider MHD flows. The numerical method is discussed in more detail in [12].

The numerical solution was obtained in a rectangular domain with a length of 35 units (measured in terms of the characteristic length L) in the streamwise direction and 20 units ($H = 20$) in the cross-stream direction. For numerical purposes, the origin was located at the bottom-left corner of the rectangular domain. It was determined that placing the center of the magnetic obstacle (i.e. the point of maximum magnetic field strength) at $x = 10$, $y = 10$, the inlet effects as well as upstream effects from the outlet could be minimized. The separation, H, between the lateral boundaries determines the solid blockage of the confined flow characterized by the blockage parameter, $\beta = 1/H$, that in this case was fixed at 5%. A distribution of 6 and 10 nodes over one unit length in the streamwise and cross-stream directions, respectively, was used with a 231×211 grid.

Boundary conditions were implemented as follows. A uniform flow in the x-direction was prescribed at the inlet, namely,

$$u = 1, \qquad v = 0. \tag{11}$$

At the outlet, Neumann conditions were used:

$$\frac{\partial u}{\partial x} = \frac{\partial v}{\partial x} = 0. \tag{12}$$

At the lateral boundaries, symmetry-type conditions simulating a frictionless wall were imposed, namely,

$$\frac{\partial u}{\partial y} = v = 0. \tag{13}$$

Finally, we assume that the induced field is zero at a long enough finite distance from the source of the applied field. Therefore, we impose that the single component of the induced field satisfies the condition

$$b_z \mid_S = 0, \tag{14}$$

where the subindex S denotes all the boundaries of the integration domain.

3.2. Results

In a previous paper [12], different flow regimes in the flow past a magnetic obstacle under conditions where inertial effects dominate over Hartmann-Rayleigh friction, were described. For the explored Reynolds numbers (100 and 200), three different flow regimes were found according to the value of the Hartmann number, namely, steady, transition and periodic vortex shedding. Here, we analyze the effect of the Hartmann-Rayleigh friction on the emergence of the instability.

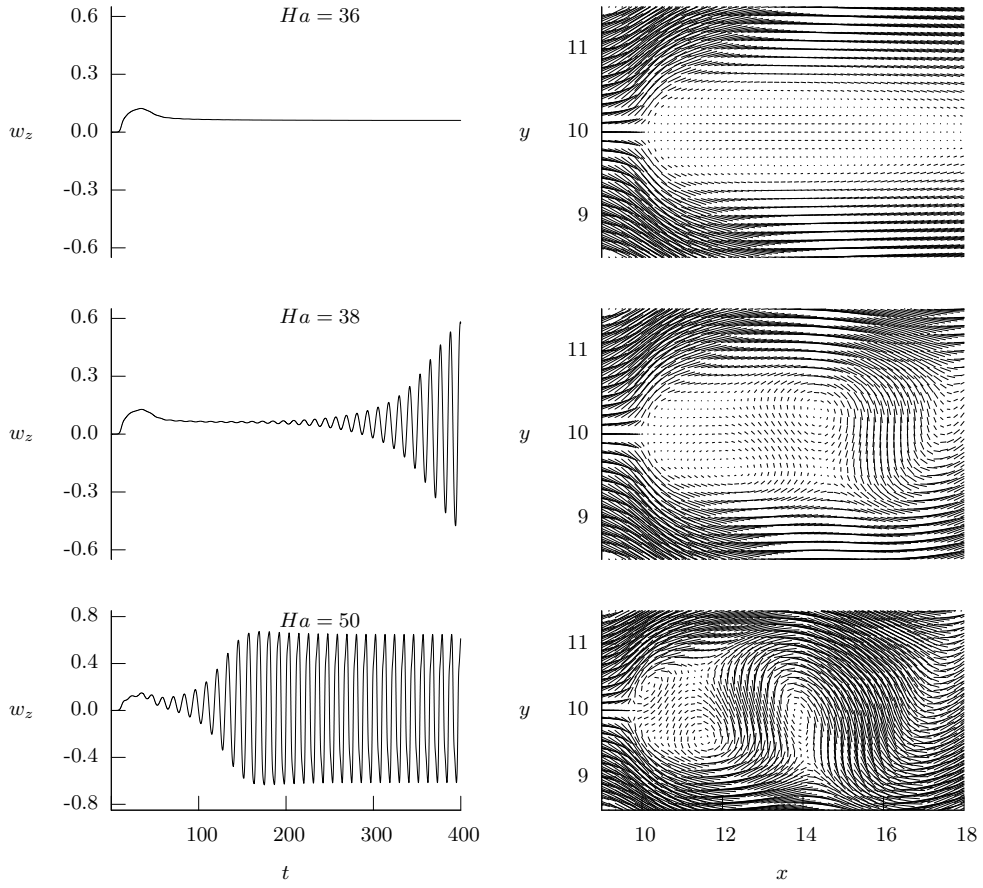

Figure 2. Vorticity as a function of time on the centerline at a distance of 15 units down stream the center of the magnetic obstacle for $Re = 200$ and different Hartmann numbers. The corresponding velocity field in the neighborhood of the magnetic obstacle is shown at the right-hand-side. Hartmann-Rayleigh friction is non-negligible. $\alpha = 1$.

The Reynolds numbers explored are 50, 100, 150 and 200, while the Hartmann number varied in the range $1 \leq Ha \leq 100$.

In general, numerical results show that the flow past a localized magnetic field presents many similarities with the flow around bluff bodies, displaying steady as well as time-periodic vortical flow regimes. Flow regimes are determined by the interplay of inertial, magnetic, and viscous forces, as well as the Hartmann-Rayleigh friction. Figure 2 shows the typical flow behavior for $Re = 200$ and different Hartmann numbers, under conditions where Hartmann-Rayleigh friction is non-negligible. In the left-hand-side, the vorticity in the mid axial line at a distance of 5 units behind the point where the magnetic field is maximum, is shown as a function of time for different Hartmann numbers. The velocity field in the near wake for the corresponding Hartmann number, is shown in the right-hand-side. For $Ha = 36$, that corresponds to a steady flow regime, the opposition to the oncoming flow in the high magnetic field zone, produces a flow around the magnetic obstacle. Shear layers parallel to the main flow direction are intensified in the lateral fringing zones and a low velocity (quasi-stagnant) region with two tenuous elongated vortices, is formed inside the obstacle and in the near wake behind it. The case $Ha = 38$ corresponds to a transition regime, where time periodic oscillations are observed at the end of a long transient

state. Sustainable self-excited wake oscillations are the signature of the onset of the instability that leads to the establishment of a vortex shedding process, similar to the classical von Kármán street. A fully established vortex shedding regime is observed when $Ha = 50$, which is reached after a very short transient time.

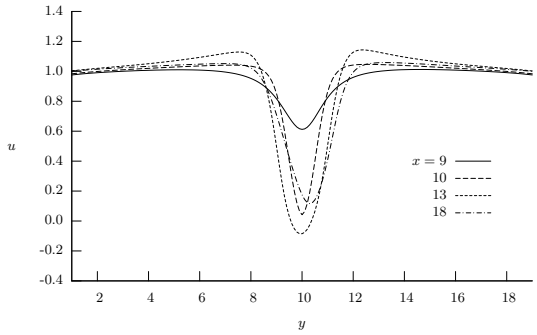

Figure 3. Axial velocity component u as a function of the transversal y-coordinate for different streamwise positions. $Re = 200$, $Ha = 38$ and $\alpha = 1$.

Figure 3 shows the axial velocity component as a function of the transversal y-coordinate, for different axial positions, when $Re = 200$, $Ha = 38$ and $\alpha = 1$. This profile clearly shows that the velocity deficit caused by the magnetic force in the localized field zone, increases with the streamwise distance, becomes maximum ($x = 13$), and then decreases ($x = 18$). Points of inflection in the profile are also observed, being more pronounced at an intermediate axial location ($x = 13$), two units downstream of the point of maximum magnetic field strength. Note that at this position, the axial velocity takes negative values, indicating the presence of recirculations. In fact, the velocity deficit across the shear layers is precisely the driving mechanism for instabilities [6, 12].

A meaningful global parameter for the characterization of flows past bluff bodies is the velocity deficit [18]. This parameter is also very helpful for the analysis of the flows under consideration. It is defined as

$$R = \frac{U_m - U_a}{U_m + U_a}, \tag{15}$$

where U_m is the velocity along the midline in the flow direction, and U_a, is the imposed inlet velocity. In the present case, $U_a = 1$. When $R = 0$, the flow is uniform; in turn, if $R = -1$, the velocity in the wake in the mid axial line is zero; on the other hand, the condition $R < -1$, means that the fluid in the midline moves in the opposite direction to the main oncoming flow, in other words, reveals the presence of recirculations. It is expected that along the wake, R will first decrease taking negative values, reach a minimum, and then increase to become zero at a sufficiently long distance downstream of the localized magnetic field.

In figure 4(a), the velocity deficit R is shown as a function of the axial coordinate for different Hartmann numbers and $Re = 200$, $\alpha = 1$. It is observed that the velocity deficit increases abruptly (i.e. R takes increasing negative values) as the flow encounters the localized magnetic field; depending on Ha, it reaches a maximum two or three units downstream of the point of maximum magnetic field strength, and decreases as the distance from the magnetic obstacle grows. Note that except for $Ha = 30$, all the other cases present recirculation, and the maximum velocity deficit is found approximately at the same axial position. However, unlike cases for $Ha = 30$, 35 and 37 that show a smooth behavior, the curve for $Ha = 38$ displays

oscillations that denote the emergence of the flow instability. In figure 4(b), the maximum value of the velocity deficit is plotted versus Ha for different Reynolds numbers. In this figure, a comparison is made between cases where the Hartmann-Rayleigh friction is negligible and those in which is not. It can be observed that for $Ha < 30$, R_{max} increases notoriously the higher the Hartmann number. However, for $Ha > 30$ the variation of R_{max} with the Hartmann number is less pronounced. In turn, the effect of Hartmann-Rayleigh friction is clearly noticed since values of R_{max} are higher (i.e. less negative) when this friction is negligible. This means that Hartmann-Rayleigh friction inhibits the flow recirculation downstream of the magnetic obstacle and smooth the shear layers.

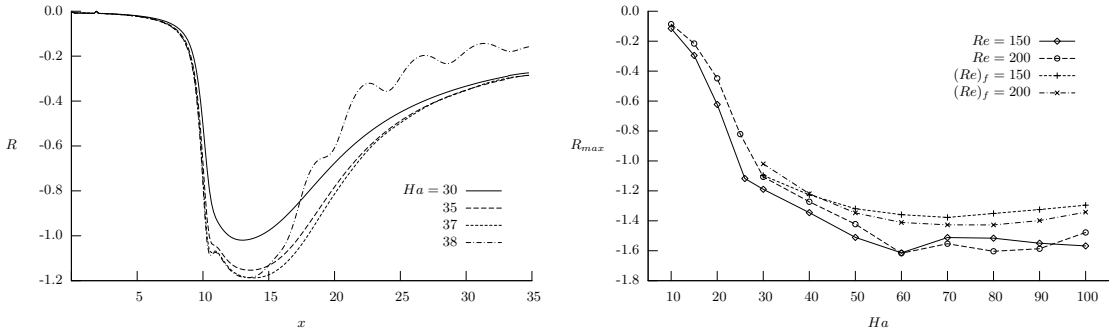

Figure 4. (a) Velocity deficit as a function of the axial coordinate for differnt Hartmann numbers. $Re = 200$, $\alpha = 1$. (b) Maximum velocity deficit as a function of the Hartmann number for different Reynolds numbers. $(Re)_f$ denotes calculations with non-negligible Hartmann-Rayleigh friction. $\alpha = 1$.

The critical conditions that trigger the flow instability, depend on the strength of inertial, viscous and magnetic forces, as well as on the Hartmann-Rayleigh friction. In figure 5(a), the critical Hartmann number is shown as a function of the Reynolds number. The solid line corresponds to conditions in which Hartmann-Rayleigh friction is absent, while dotted line accounts for cases where this friction is non-negligible. For practical purposes, Ha_{crit} was detected by fixing the Reynolds number and varying slightly the Hartmann number until sustained time-oscillations of the vorticity in the wake behind the obstacle are found. In the absence of friction, Ha_{crit} is essentially the same (≈ 25) for $Re = 50$ and 100. When Re increases to 150 and 200, Ha_{crit} increases to 26 and 28, respectively. This shows that increasing inertia, a stronger magnetic force is needed to destabilize the flow. For the case when Hartmann-Rayleigh friction is not neglected, the flow does not show unstable behavior for $Re = 50$ and 100, within the explored range of Hartmann numbers. Sustainable time-oscillations are observed only for $Re = 150$ and 200 and Ha_{crit} raises to 38.5 and 38, respectively. As expected, the influence of the Hartmann-Rayleigh friction delays the appearance of instabilities. This means that under the influence of friction, for the same Reynolds number, higher Hartmann numbers are required for destabilizing the flow, compared to cases where the friction is negligible. The interaction parameter is also a useful dimensionless number for the characterization of critical conditions. It is defined as $N = \sigma B_{max}^2 L/\rho U = Ha^2/Re$, and estimates the magnitude of magnetic forces compared with inertial forces. In figure 5(b), the critical interaction parameter is shown as a function of the Reynolds number. It is observed that N_{crit} decreases as the Reynolds number grows. Under the influence of friction, for the cases where the instability is not inhibited ($Re = 150$ and 200), N_{crit} takes higher values than those found when the friction is absent. Previous results show that Hartmann-Rayleigh friction acts as an stabilizing factor and, under certain conditions, may inhibit the emergence of flow instabilities.

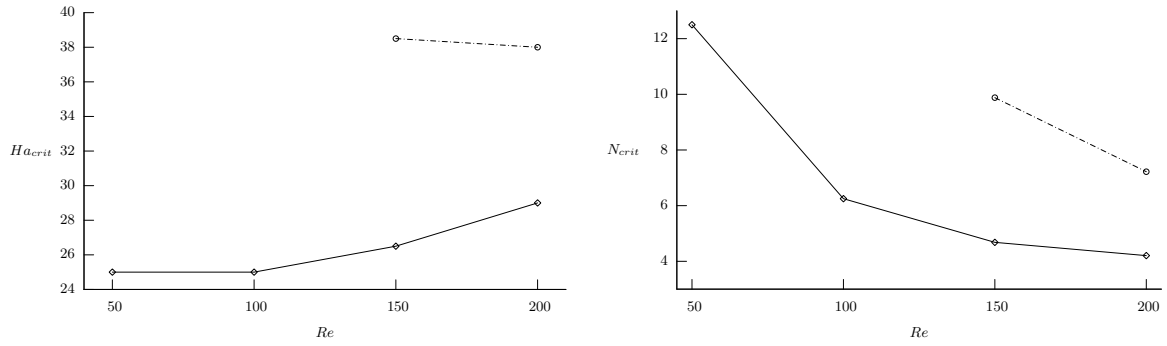

Figure 5. (a) Critical Hartmann number for the appearance of the instability as a function of the Reynolds number. (b) Critical interaction parameter as a function of the Reynolds number. Solid line corresponds to flow conditions where Hartmann-Rayleigh friction is negligible. Dotted line shows the effect of Hartmann-Rayleigh friction. $\alpha = 1$.

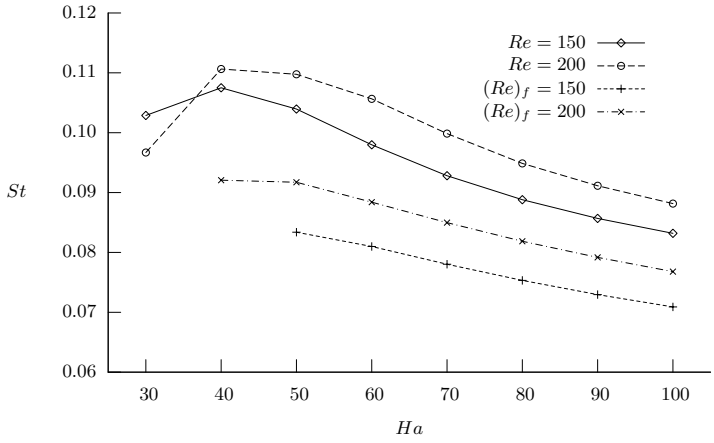

Figure 6. Strouhal number as a function of the Hartmann number. $(Re)_f$ denotes calculations with non-negligible Hartmann-Rayleigh friction. $\alpha = 1$.

The vortex shedding in the wake behind the magnetic obstacle, is characterized through the Strouhal number, defined as,

$$St = \frac{fL}{U}, \tag{16}$$

where f is the shedding frequency. The Strouhal number was determined from the fluctuating values of the vorticity in the wake behind the obstacle. In figure 6, the Strouhal number as a function of the Hartmann number is shown for $Re = 150$ and 200 both with and without Hartmann-Rayleigh friction. The Strouhal number exhibits a weak dependence on Ha, similarly to the behaviour observed in other MHD flows where vortex shedding phenomenon appears [3, 6]. For cases with negligible friction, St rises up to a maximum value and thereafter presents a slight decrease with Ha. The maximum values reached by St are 0.107 and 0.111 for $Re = 150$ and 200, respectively. In turn, under the influence of Hartmann-Rayleigh friction, the maximum values reached by St for the same Reynolds numbers are 0.082 and 0.093; from these values, a slight decrease with Ha is also observed. Cleraly, the effect of Hartmann-Rayleigh friction is to

reduce the Strouhal number as a result of the additional damping mechanism.

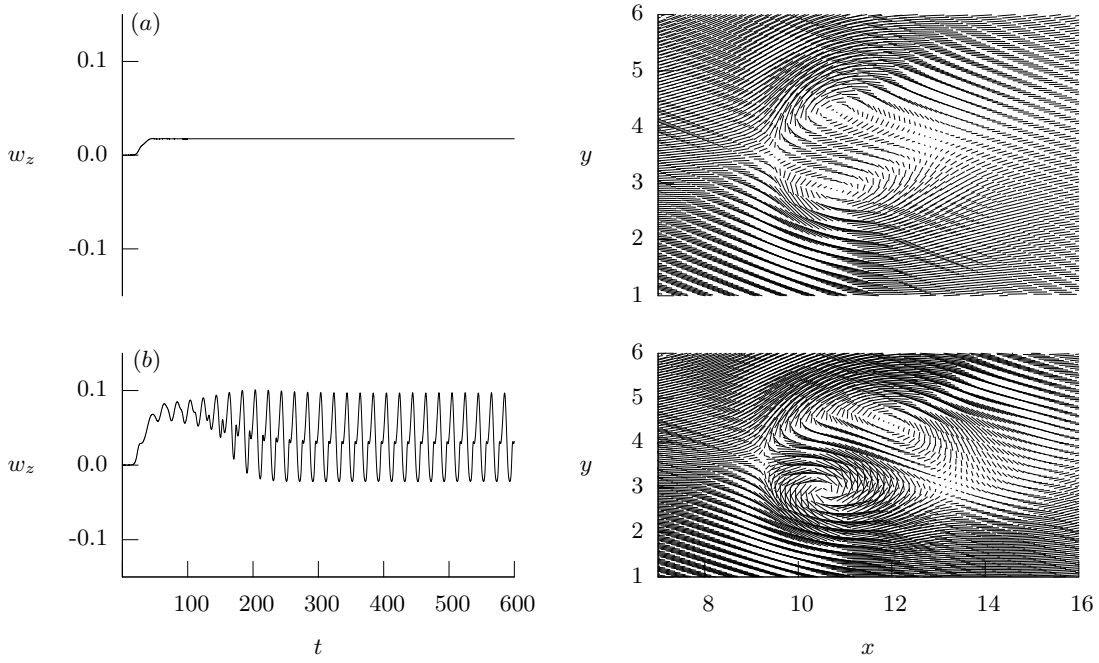

Figure 7. Vorticity as a function of time on the centerline at a distance of 5 units downstream of the center of the magnetic obstacle for $Ha = 0.9$ and $\alpha = 0.167$. The corresponding velocity field in the neighborhood of the magnetic obstacle is shown at the right-hand-side. (a) $Re = 700$, $I = 605$; (b) $Re = 1000$, $I = 1135$.

4. Flows under the influence of injected electric currents

Let us now consider the flow past a localized magnetic field when an external electric current is injected to the thin fluid layer in the negative y-direction. Under these conditions, the governing equations are modified to take into account the additional force created by the interaction of the injected current with the localized field. In dimensionless terms, the governing equations take the form:

$$\frac{\partial u}{\partial x} + \frac{\partial v}{\partial y} = 0, \tag{17}$$

$$\frac{\partial u}{\partial t} + \left(u\frac{\partial u}{\partial x} + v\frac{\partial u}{\partial y}\right) K = -\frac{\partial p}{\partial x} + \frac{1}{Re}\nabla_\perp^2 u - \frac{u}{\tau} + \frac{Ha^2}{Re} I(j_y B_z^0 - B_z^0), \tag{18}$$

$$\frac{\partial v}{\partial t} + \left(u\frac{\partial v}{\partial x} + v\frac{\partial v}{\partial y}\right) K = -\frac{\partial p}{\partial y} + \frac{1}{Re}\nabla_\perp^2 v - \frac{v}{\tau} - \frac{Ha^2}{Re} I\, j_x B_z^0, \tag{19}$$

$$\nabla_\perp^2 b_z - u\frac{\partial B_z^0}{\partial x} - v\frac{\partial B_z^0}{\partial y} = 0, \tag{20}$$

$$\frac{\partial b_z}{\partial y} = I\, j_x, \qquad -\frac{\partial b_z}{\partial x} = I\, j_y, \tag{21}$$

where the induced and injected electric current densities have been normalized by the magnitude of the injected current density J_0. The normalization of all the other variables remains the same as in Section 3. In addition to the Hartmann and Reynolds numbers, we have a new dimensionless parameter, $I = J_0/\sigma U B_{max}$ which is the ratio of injected to induced electric currents. The parameters K and τ^{-1} have the same form as equations (7)-(8) but the local Hartmann number is given by $\mathcal{H}a(x,y) = HaB_z^0\sqrt{I}$.

The system of equations (18)-(21) was solved numerically using boundary conditions (11)-(14) and some parameters were close to those used in the experiments by Honji and Haraguchi [10]. A full comparison with the experiments is not possible since the information provided is not complete. We estimated that in the experiments the Hartmann number was approximately $Ha \approx 0.9$, the dimensionless layer thickness was $\alpha = 0.167$, and the blockage parameter β was 14%. We used these parameters for two different cases, namely, a) $Re = 700$, $I = 605$, and b) $Re = 1000$, $I = 1136$. Since $I >> 1$, a considerable Lorentz force is obtained although the Hartmann number used is much smaller that those used in Section 3. Figure 7 shows, for both cases, the vorticity as a function of time on the centerline at a distance of 5 units downstream of the point of maximum magnetic field intensity. The corresponding velocity field in the neighborhood of the magnetic obstacle is also shown at the right-hand-side. In case a) a steady vortex dipole was found, while in case b), numerical results show a vortex shedding in the wake behind the magnetic obstace, with an Strouhal number equal to 0.05. Similar flow patterns were found in the experiments made by Honji and Haraguchi, however, a quantitative comparison is not possible with the information at hand. Anyway, numerical simulations are able to grasp the main characteristic features of the experimental situation. A complete assessment of the numerical model requires additional experimental data.

5. Conclusions

We analyzed the effect of Hartmann-Rayleigh friction in the emergence of instabilities in the flow past a localized magnetic field. In the absence of friction, flow regimes are only determined by the interplay of inertial, magnetic, and viscous forces in the bulk of the flow. Under certain conditions, shear layers created by the opposition of Lorentz force to the oncoming flow, may become unstable. The velocity deficit across the shear layers is the driving mechanism for instabilities. In this context, Hartmann-Rayleigh friction acts as an stabilizing factor, delaying the appearance of instabilities to larger values of the Hartmann number for a given Reynolds number. In some cases, Hartmann-Rayleigh friction may completely inhibit the emergence of flow instabilities. Its effect is also manifested in a reduction of the Strouhal number, compared to cases where the friction is negligible. Further numerical and experimental work is necessary to improve the description and understanding of flows in localized magnetic fields when electric currents are injected in a thin fluid layer. Nevertheless, the present numerical simulations retain important features observed experimentally,

Acknowledgments

Support form UC MEXUS-CONACYT and DGAPA-UNAM under project IN111705 is also gratefully acknowledged.

References

[1] Reed C B and Picologlou B F 1989 Side wall flow instabilities in liquid-metal flow under blanket relevant conditions, *Fusion Techn.* **15** 705–715

[2] Burr U, Barleon L, Müller U and Tsinober A 2000 Turbulent transport of momentum and heat in magnetohydrodynamic rectangular duct flow with strong side wall jets, *J. Fluid Mech.* **406** 247–279

[3] Mück B, Günther C, Müller U and Bühler L 2000 Three-dimensional MHD flows in rectangular ducts with internal obstacles. *J. Fluid Mech.* **418** 265–295

[4] Frank M, Barleon L and Müller U 2001 Visual analysis of two-dimensional magnetohydrodynamics *Phys. Fluids* **13** 2287–95
[5] Alpher A, Hurwitz H, Johnson R H and White D R 1960 Some studies of free-surface mercury magnetohydrodynamics *Rev. Mod. Phys.* **32** 758-769
[6] Bühler L 1996 Instabilities in quasi-two-dimensional magnetohydrodynamic flows *J. Fluid Mech.* **326** 125–150
[7] Hansen A E, Marteau D and Tabeling P 1998 Two-dimensional turbulence and dispersion in a freely decaying system, *Phys. Rev. E*, **58** 7261–71
[8] Rothstein D, Henry E and Gollub J P 1999 Persisntent patterns in transient chaotic fluid mixing Nature **401** 770–772
[9] Honji H 1991 Wavy wake formation in the absence of submerged bodies in electrolyzed salt water *J. Phys. Soc. Japan* **60** 1161–64
[10] Honji H and Haraguchi Y 1995 Electrolytically induced quasi-two dimensional vortex pairs *J. Phys. Soc. Japan* **64**, 2274–77
[11] Afanasyev Y D and Korabel V N 2006 Wakes and vortex streets generated by translating force and force doublet: laboratory experiments *J. Fluid Mech* **553** 119–141
[12] Cuevas S, Smolentsev S and Abdou M 2006 On the flow past a magnetic obstacle *J. Fluid Mech* **553** 227–252
[13] Davidson P A 2001 *Introduction to magnetohydrodynamics* (Cambridge: Cambridge University Press)
[14] McCaig M 1977 *Permanent magnets in theory and practice*, (New York: Wiley).
[15] Smolentsev S 1997 Averaged model in MHD duct flow calculations *Magnetohydrodynamics* **33**(1) 42–47
[16] Lavrent'ev I V, Molokov S Yu, Sidorenkov S I and Shishko A R 1990 Stokes flow in a rectangular magnetohydrodynamic channel with nonconducting walls within a nonuniform magnetic field at large Hartmann numbers *Magnetohydrodynamics* **26**(3) 328–338
[17] Griebel M, Dornseifer T and Neunhoeffer T 1998 *Numerical simulation in fluid dynamics* (New York: SIAM)
[18] Chen D and Jirka H G 1997 Absolute and convective instabilities of plane turbulent wakes in shallow water layer *J. Fluid Mech* **338** 157–172